catalysts

MDPI

Supplementary Materials

Low Temperature Ozonation of Acetone by Transition Metals Derived Catalysts: Activity and Sulfur/Water Resistance

Peixi Liu [1], Lichun Chen [1], Hairong Tang [2], Jiaming Shao [1,3], Fawei Lin [4], Yong He [1], Yanqun Zhu [1] and Zhihua Wang [1,*]

[1] State Key Laboratory of Clean Energy Utilization, Zhejiang University, Hangzhou 310027, China
[2] Nuclear Power Insitute of China, Chengdu 610041, China
[3] Zhejiang SUPCON Technology Co., Ltd., Hangzhou 310053, China
[4] School of Environmental Science and Engineering, Tianjin University, Tianjin 300072, China
* Correspondence: wangzh@zju.edu.cn

Citation: Liu, P.; Chen, L.; Tang, H.; Shao, J.; Lin, F.; He, Y.; Zhu, Y.; Wang, Z. Low Temperature Ozonation of Acetone by Transition Metals Derived Catalysts: Activity and Sulfur/Water Resistance. *Catalysts* **2022**, *12*, 1090. https://doi.org/10.3390/catal12101090

Academic Editors: Antonia Iazzetti and Alessia Ciogli

Received: 18 August 2022
Accepted: 16 September 2022
Published: 21 September 2022

Publisher's Note: MDPI stays neutral with regard to jurisdictional claims in published maps and institutional affiliations.

1. NH_3-TPD

NH_3-TPD is a common characterization method to investigate the surface acidity of catalysts, in which, usually, NH_3 desorption peaks in the temperature range 100~280 °C refer to weak acid sites, and desorption peaks in 280~450 °C, 450~750 °C, signify moderate acid sites and strong acid sites, respectively. Among those, weak and moderate acid sites usually indicate physically adsorbed NH_3 and partial ionic NH_4^+, corresponding to Lewis acid sites, whereas strong acid sites refer to desorption of coordinated NH_3 corresponding to Brönsted acid sites [1–3]. It is widely accepted that Lewis acid sites are applied to the decomposition of ozone and production of active oxygen species, while Brönsted acid sites mainly act on adsorption of VOCs on the surface of catalysts [1,2]. As a result, both Lewis and Brönsted acid sites are beneficial and significant for catalytic ozonation of VOCs. From Figure S1 (a), in temperature ranges 100~280 °C and 280~450 °C, NH_3 desorption peaks area over different active component catalysts decreased in the order of Mn1.5% > Co1.5% > Cr1.5% > Fe1.5% > Al_2O_3, which stood for the larger amounts of Lewis acid sites of Mn1.5% and Co1.5% catalysts. As for Brönsted acid sites, it was obvious that in higher temperatures 450~650 °C, Al_2O_3 possessed the largest desorption peaks area, besides, Co1.5% took the second place. The total acid sites amounts of those catalysts decreased in the sequence of Mn1.5% > Co1.5% > Cr1.5% > Al_2O_3 > Fe1.5%. In Figure S1 (b), Lewis acid sites amounts of CrO_x/Al_2O_3 followed the sequence of Cr5% > Cr1.5% > Cr2.5% >Al_2O_3, whereas Al_2O_3 still possessed most Brönsted acid sites. The total acid sites amounts of CrO_x/Al_2O_3 decreased in the order of Cr5% > Cr1.5% > Al_2O_3 > Cr2.5%. In general, above different active components catalysts and different Cr loading mass fraction catalysts, the impregnation of active transition metal oxides mainly increased the Lewis acid sites, meanwhile decreasing Brönsted acid sites. Lewis acid sites increased with the mass fraction of Cr in CrO_x/Al_2O_3, except for Cr2.5%. Generally, more acid sites would improve the adsorption and activation of VOCs [1,3], but the sequence of acid sites amounts fitted with that of catalytic activities on acetone removal not so well. The results meant the acid sites of catalysts were not the only influence factor on catalytic activities, therefore further characterization investigation on those different catalysts remained to be carried out.

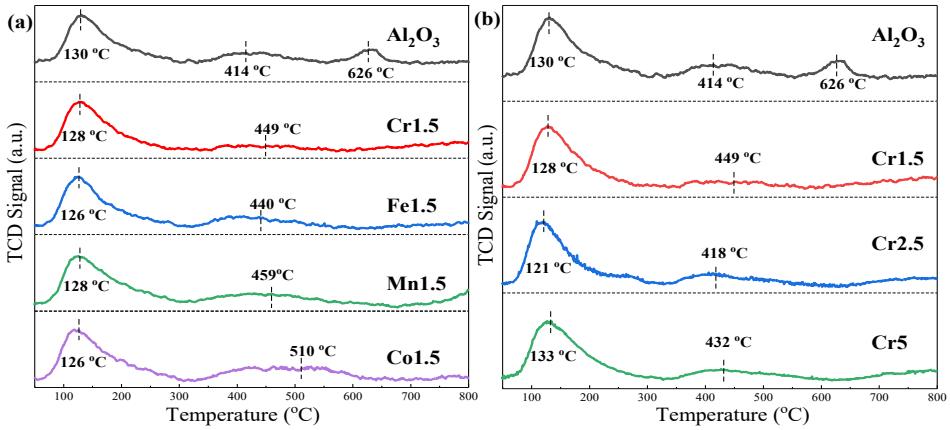

Figure S1. The NH_3-TPD profiles of different catalysts. (**a**) MO_x/γ-Al_2O_3 (M = Cr/Fe/Mn/Co); (**b**) Cr1.5~5%.

2. CO_2-TPD

Carbonate species are crucial intermediates during catalytic ozonation of the carbonaceous compound acetone, deposition of which would block or occupy active sites, hence causing the deactivation of catalysts [4]. The CO_2-TPD characterization is widely utilized to explore the carbonate species desorption ability of catalysts. From the curves in Figure S2 (a) and (b), γ-Al_2O_3 support showed the strongest CO_2 desorption peak at low temperature ~127 °C, which demonstrated that desorption of CO_2 mainly occurred on the surface of the support, with abundant oxygen defects [5]. The loss of adsorption volume after metal oxides impregnation may be ascribed to the coverage of metal oxides [5]. But over those catalysts, in the low-temperature range, all CO_2-TPD curves exhibited a desorption peak around the reaction temperature of 120 °C, indicating that carbonate species could effectively decompose and products CO_2 could be timely desorbed during the catalytic ozonation process [1,4].

Over Cr1.5% catalysts, two desorption peaks at 124 °C and 376 °C were observed, with temperatures lower than those of other catalysts, except for Co1.5% at 117 °C and 415 °C. Generally speaking, lower peaks temperature indicated higher CO_2 selectivity [1]. But from activity evaluation results, Cr1.5% exhibited the highest catalytic activity and CO_2 selectivity, rather than Co1.5%, which may be ascribed to the inferior of less surface area and adsorption ability of Co1.5%. But over three CrO_x/Al_2O_3 catalysts, the smaller peaks area and higher peaks temperature of Cr1.5% were unsatisfactory, compared to Cr2.5% and Cr5%, which also illustrated that, in CrO_x/Al_2O_3 catalysts, desorption ability of CO_2 was not the decisive factor during the whole catalytic ozonation process.

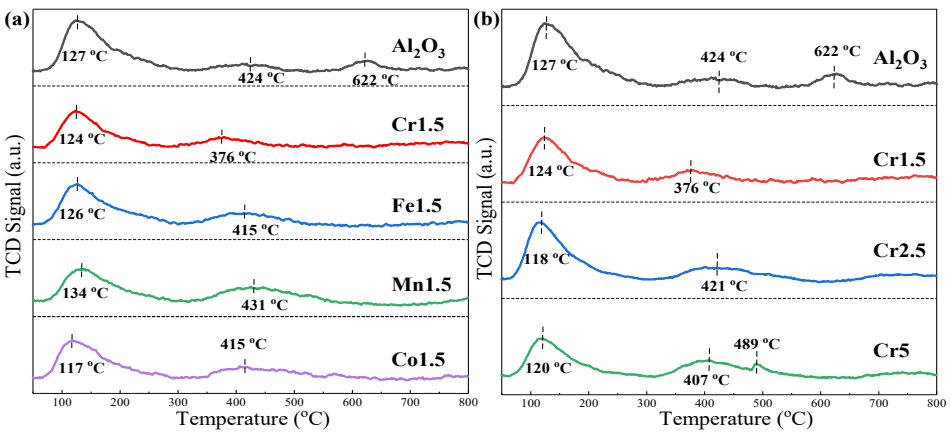

Figure S2. The CO_2-TPD profiles of different catalysts. (**a**) MO_x/γ-Al_2O_3 (M = Cr/Fe/Mn/Co); (**b**) Cr1.5~5%.

3. C_3H_6O-TPD

The C_3H_6O-TPD was utilized here to explore surface acetone adsorption sites and estimate acetone adsorption ability of catalysts [6]. From Figure S3 (a), the first desorption peaks over all catalysts appeared at low temperature ~120 °C, while the peak area of Cr1.5% at 120 °C was not extraordinarily high, thus it was deduced that adsorption of acetone on Cr1.5% was not the most critical step in the whole catalytic ozonation process over Cr1.5%. But we could infer that the adsorption and activation of acetone on Co1.5% limited its catalytic activity. However, in Figure S3 (b), with more Cr impregnated, the first peak temperatures of Cr2.5% and Cr5% shifted to lower temperature ~117 °C, demonstrating that Cr impregnation could improve desorption of C_3H_6O, but the peak areas under low temperature of Cr2.5% and Cr5% were smaller than those of Cr1.5% and γ-Al_2O_3 support, which illustrated that excessive Cr would be adverse to adsorption of C_3H_6O [7], maybe furthermore imposing negative influence on their catalytic activity performance.

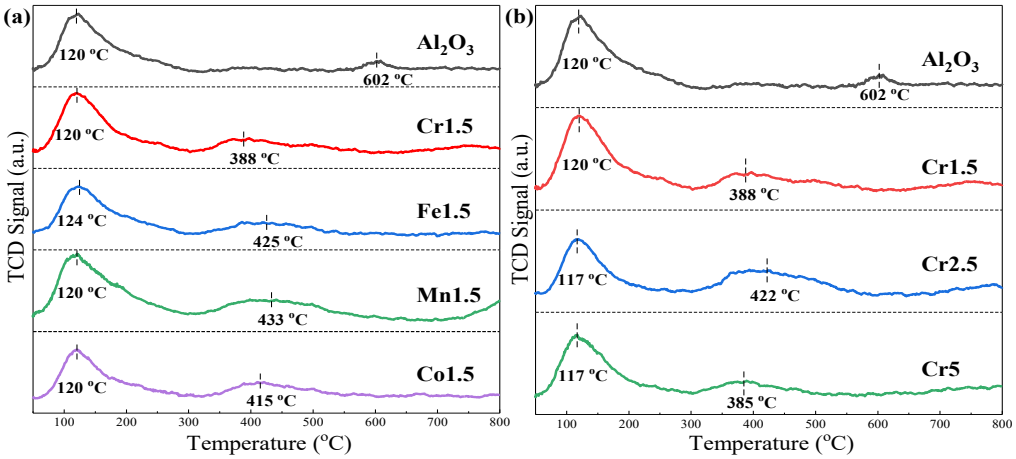

Figure S3. The C_3H_6O-TPD profiles of different catalysts. (**a**) MO_x/γ-Al_2O_3 (M = Cr/Fe/Mn/Co); (**b**) Cr1.5~5%.

4. O_2-TPD

The O_2-TPD is also commonly utilized to estimate adsorption ability of oxygen and mobility ability of oxygen species over catalysts [1,4]. In O_2-TPD curves, desorbed oxygen species are usually divided as chemically desorbed oxygen, surface lattice oxygen and bulk lattice oxygen, according to desorption temperature from low to high [4,6]. Generally, desorption peaks of oxygen under 300 °C are ascribed to release of chemically desorbed oxygen and active surface oxygen, while in the temperature range of 300~600 °C and above 600 °C, desorption peaks state liberation of subsurface and lattice oxygen [1,6]. From Figure S4 (a), over γ-Al_2O_3 support, two obvious desorption peaks were observed, at 409 °C and 618 °C, which symbolized surface lattice oxygen and bulk lattice oxygen, respectively. Once transition metal oxides were impregnated, desorption peaks at low temperature 100~250 °C appeared, and the peak at higher temperature 618 °C disappeared, which demonstrated generation of more oxygen vacancies for mobility of chemically adsorbed oxygen, and the decrease of oxygen vacancies of bulk lattice oxygen. It was declared by J. M. Shao and F. W. Lin that more chemically adsorbed oxygen would be advantageous and crucial for activation and catalytic ozonation of VOCs [1,4]. Cr1.5% owned the largest desorption peak area and the lowest desorption temperature at 150 °C, which illustrated the most chemically adsorbed oxygen, easier activation and higher mobility [6], in addition, consistent with its best catalytic activity on acetone conversion. While, in Figure S4 (b), among three CrO_x/Al_2O_3, Cr2.5% possessed the largest desorption peak area and the lowest desorption temperature at 118 °C, followed by Cr5%, and last Cr1.5%. It meant chemically absorbed oxygen amounts followed the sequence of Cr2.5%

> Cr5% > Cr1.5%, which could compensate for the lack of acid sites over Cr2.5% catalysts. Spent catalysts Cr1.5% were also compared with fresh Cr1.5% in O_2-TPD curves in Figure S4 (c), it could be seen that after catalytic ozonation experiments, all three Cr1.5% spent produced more oxygen vacancies for chemically adsorption of oxygen and surface lattice oxygen. Especially after SO_2-resistance experiments, a conspicuous increase of surface lattice oxygen and bulk lattice oxygen was observed, which could illustrate that SO_2 influence on catalysts Cr1.5% was mainly transferring active oxygen species into lattice oxygen in catalysts, and enhanced difficulty to diffuse into the gas phase for catalytic ozonation process [6]. It was reported that more O species could be produced by the collision between H_2O and dissociated electrons [8,9]. But because of larger polarity and a stronger affinity with catalysts surface of H_2O, competition adsorption between H_2O and acetone molecules and blocking active sites would cause an inhibition effect on acetone removal efficiency [9].

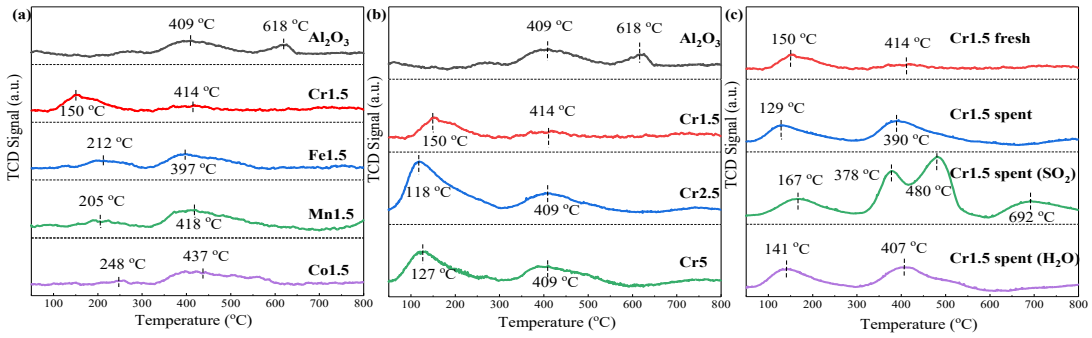

Figure S4. The O_2-TPD profiles of different catalysts. (**a**) MO_x/γ-Al_2O_3 (M = Cr/Fe/Mn/Co); (**b**) Cr1.5~5%; (c) Cr1.5% spent.

5. H_2-TPR

In Figure S5 (a) H_2-TPR curves, for Cr1.5%, two reduction peaks at 376 °C and 576 °C, belonged to the reduction peaks of Cr^{6+} to Cr^{3+} and highly dispersed Cr_2O_3 [10,11]. For Cr1.5%, the lower temperature at 376 °C with relatively more H_2 consumption, demonstrated the superiority of its low-temperature reducibility and catalytic activity, and easier desorption of adsorbed oxygen species connected with Cr ions, contributing to its highest decomposition efficiency of acetone [1,12,13]. From the view of Figure S5 (b), with the increase of Cr mass fraction over catalysts, the H_2 consumption became larger, illustrating the increase of oxidation sites [1,14,15]. Catalyst Cr1.5% exhibited higher activity, with lower H_2 consumption and higher reduction temperature over three CrO_x/γ-Al_2O_3, which was consistent with the description in literature [16] that a small number of oxidation sites with low activity and weak interaction between active components and supports were beneficial to decomposition of ozone and VOCs. H_2 consumptions over three CrO_x/γ-Al_2O_3 were not completely consistent with their activity order, because redox ability and acidity integratedly affected catalytic activity [10,11]. From the characterization results of Figure S5 (c), for Cr1.5% spent and Cr1.5% spent (SO_2) catalysts, reduction peaks temperatures shifted to 386 °C and 540 °C, compared to 376 °C for Cr1.5% fresh catalyst, which provided evidence of enhancement of Cr-O bond strength and accumulation of carbonates and sulfates on the catalysts surface, after catalytic reaction and SO_2-resistance catalytic reaction [1,10,15]. Combining with characterization and analysis results of XPS that Cr^{6+} was the main active substance, it could also be discovered that peaks area for reduction decreased after catalytic reaction and SO_2/H_2O-resistance catalytic reaction, which could be deduced that deactivation of Cr1.5% catalysts may result from the loss of Cr^{6+}.

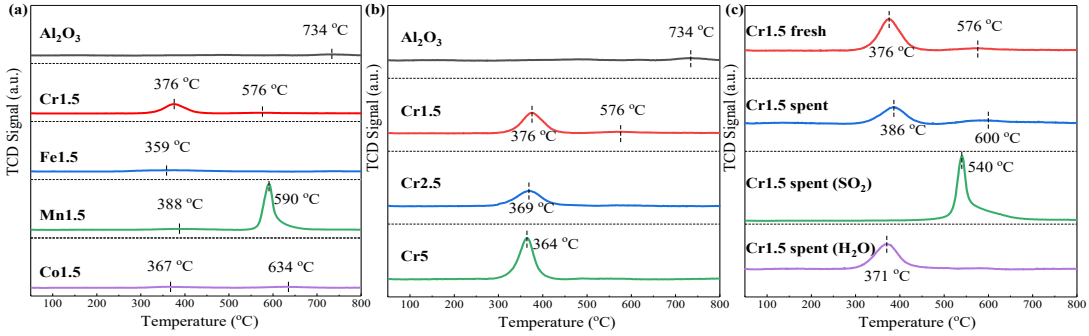

Figure S5. The H_2-TPR profiles of different catalysts. (**a**) MO_x/γ-Al_2O_3 (M = Cr/Fe/Mn/Co); (**b**) Cr1.5~5%; (**c**) Cr1.5% spent.

6. SEM-EDS

Figure S6 exhibited SEM-EDS (scanning electron microscope energy dispersive spectrometer) mappings of different catalysts. As shown, the elemental mapping mainly reflected the Al and O elements, which could be ascribed to the γ-Al_2O_3 support of those catalysts. The element fractions of transition metals (Cr/Fe/Mn/Co) were quite lower, but the homogeneous distribution of all elements including Al/O/Cr/Fe/Mn/Co can still be observed, demonstrating the success of impregnation and good dispersion of active components. And the results of ICP-OES (inductively coupled plasma optical emission spectroscopy) listed in Table S1 could also prove the presence of active components, which were close to the theoretical mass fractions of 1.5%.

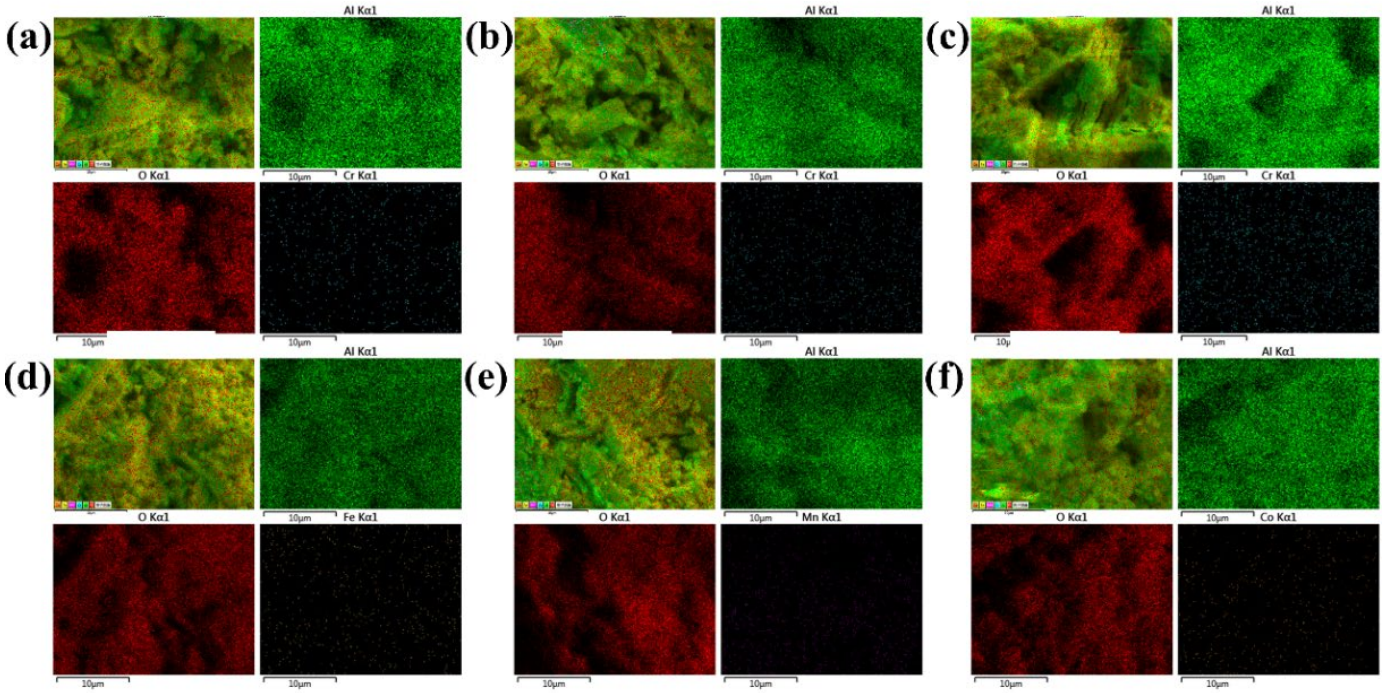

Figure S6. SEM-EDS mappings of different catalysts. (**a**) Cr1.5%/γ-Al_2O_3; (**b**) Cr2.5%/γ-Al_2O_3; (**c**) Cr5%/γ-Al_2O_3; (**d**) Fe1.5%/γ-Al_2O_3; (**e**) Mn1.5%/γ-Al_2O_3; (**f**) Co1.5%/γ-Al_2O_3.

Table S1. Metals loadings in catalysts.

Catalysts	Metals loading (wt.%)
Al_2O_3	—
Fe1.5%	1.37
Mn1.5%	1.45
Co1.5%	1.45
Cr1.5%	1.49

7. Ozone decomposition

Ozone decomposition performance of different catalysts were measured, results illustrated in Figure S7. Results demonstrated that ozone decomposition performance of Fe1.5%, Mn1.5%, Co1.5% were excellent, nearly close to 100% decomposition efficiencies, which were higher than 60% of Cr1.5%. And with the increase of Cr fraction, the ozone decomposition performance became inferior, with 40% conversion of Cr5% catalyst, which was consistent with the trend of acetone removal on those CrO_x/γ-Al_2O_3. By comparison with Figure 5 (d) in the manuscript, it could be concluded that without acetone, ozone decomposition might be inhibited, which can be ascribed to the lack of reaction process between acetone and ozone molecules, resulting the unsatisfactory ozone decomposition performance. And it can also be deduced that too fast ozone decomposition rates could also be a disadvantage for acetone removal, because of unmatched reaction rates.

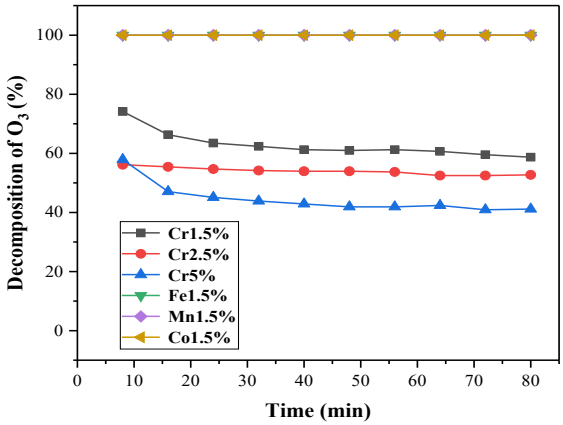

Figure S7. Decomposition efficiencies of ozone by different catalysts, without acetone.

References

1. Shao, J.; Lin, F.; Wang, Z.; Liu, P.; Tang, H.; He, Y.; Cen, K. Low temperature catalytic ozonation of toluene in flue gas over Mn-based catalysts: Effect of support property and SO_2/water vapor addition, *Appl. Catal. B.* **2020**, *266*, 118662. https://doi.org/10.1016/j.apcatb.2020.118662.
2. He, D.; Liu, L.; Ren, J.; Hu, T. Catalytic combustion of volatile organic compounds over CuO-CeO_2 supported on SiO_2-Al_2O_3 modified glass-fiber honeycomb, *J. Fuel Chem. Technol.*, **2017**, *45*, 354–361. https://doi.org/10.1016/S1872-5813(17)30020-8.
3. Gao, J.; Guo, J.; Liang, D.; Hou, Z.; Fei, J.; Zheng, X. Production of syngas via autothermal reforming of methane in a fluidized-bed reactor over the combined CeO_2-ZrO_2/SiO_2 supported Ni catalysts, *Int. J. Hydrog. Energ.* **2008,** *33,* 5493–5500. https://doi.org/10.1016/j.ijhydene.2008.07.040
4. Zhang, Z.; Xiang, L.; Lin, F.; Wang, Z.; Yan, B.; Chen, G. Catalytic deep degradation of Cl-VOCs with the assistance of ozone at low temperature over MnO_2 catalysts. *Chem. Eng. J.* **2021**, *426*, 130814, https://doi.org/10.1016/j.cej.2021.130814.
5. Lin, F.; Jiang, X.; Boreriboon, N.; Wang, Z.; Song, C.; Cen, K. Effects of supports on bimetallic Pd-Cu catalysts for CO_2 hydrogenation to methanol. *Appl. Catal. A- Gen*, **2019**, *585*, 117210. https://doi.org/10.1016/j.apcata.2019.117210.
6. Yang, H.-H.; Du, J.; Wu, M.; Zhou, H.; Yi, X.; Zhan, J.; Liu, Y. Tin-modified α-MnO_2 catalyst with high performance for benzene oxidation, ozone decomposition and particulate matter filtration. *Chem. Eng. J.* **2022**, *427*, 132075. https://doi.org/10.1016/j.cej.2021.132075
7. Meng, F.; Zhang, S.; Zeng, Y.; Zhang, M.; Zou, H.; Zhong, Q.; Li, Y. Promotional effect of surface fluorine on TiO_2: Catalytic conversion of O_3 and H_2O_2 into ·OH and $\cdot O_2^-$ radicals for high-efficiency NO oxidation. *Chem. Eng. J.* **2021**, *424*, 130358, https://doi.org/10.1016/j.cej.2021.130358. .

8. Raju, B. R.; Reddy, E. L.; Karuppiah, J.; Reddy, P. M. K.; Subrahmanyam, C. Catalytic non-thermal plasma reactor for the decomposition of a mixture of volatile organic compounds, *J. Chem. Sci*. **2013**, *125*, 673–678. https://doi.org/10.1007/s12039-013-0401-2.
9. Rochard, G.; Olivet, L.; Tannous, M.; Poupin, C.; Siffert, S.; Cousin, R. Recent Advances in the Catalytic Treatment of Volatile Organic Compounds: A Review Based on the Mixture Effect. *Catalysts* **2021**, *11*, 1218, https://doi.org/10.3390/catal11101218.
10. Su, J. Experimental study on catalytic oxidation of DCM over HZSM-5 supported transition metal oxides, Zhejiang University: Hangzhou, China, 2016.
11. Yang, P.; Shi, Z.; Tao, F.; Yang, S.; Zhou, R. Synergistic performance between oxidizability and acidity/texture properties for 1,2-dichloroethane oxidation over (Ce,Cr)xO_2/zeolite catalysts. *Chem. Eng. Sci.* **2015**, *134*, 340–347, https://doi.org/10.1016/j.ces.2015.05.024.
12. Wang, Z.; Liu, Y.; Yang, T.; Deng, J.; Xie, S.; Dai, H. Catalytic performance of cobalt oxide-supported gold-palladium nanocatalysts for the removal of toluene and o -xylene. *Chin. J. Catal.* **2017**, *38*, 207–216, https://doi.org/10.1016/s1872-2067(16)62569-x.
13. Bai, B.; Li, J.; Hao, J. 1D-MnO_2, 2D-MnO_2 and 3D-MnO_2 for low-temperature oxidation of ethanol. *Appl. Catal. B*. **2015**, *164*, 241–250. https://doi.org/10.1016/j.apcatb.2014.08.044.
14. Sun, M.; Li, W.; Zhang, B.; Cheng, G.; Lan, B.; Ye, F.; Zheng, Y.; Cheng, X.; Yu, L. Enhanced catalytic performance by oxygen vacancy and active interface originated from facile reduction of OMS-2. *Chem. Eng. J.* **2018**, *331*, 626–635, https://doi.org/10.1016/j.cej.2017.09.028.
15. Zhu, G.; Zhu, J.; Jiang, W.; Zhang, Z.; Wang, J.; Zhu, Y.; Zhang, Q. Surface oxygen vacancy induced α-MnO_2 nanofiber for highly efficient ozone elimination. *Appl. Catal. B*. **2017**, *209*, 729–737. https://doi.org/10.1016/j.apcatb.2017.02.068.
16. Long, L.; Zhao, J.; Yang, L.; Fu, M.; Wu, J.; Huang, B.; Ye, D. Room temperature catalytic ozonation of toluene over MnO_2/Al_2O_3. *Chinese J. Catal*. **2011**, *32*, 904–916. https://doi.org/10.1016/S1872-2067(10)60216-1.